Nuclear tunneling and dynamical Jahn-Teller effect in graphene with vacancy

Z. S. Popović, B. R. K. Nanda, and S. Satpathy

Phys. Rev. B **86**, 085458 — Published 30 August 2012

DOI: 10.1103/PhysRevB.86.085458

Nuclear Tunneling and Dynamical Jahn-Teller Effect in Graphene with Vacancy

Z. S. Popović*, B. R. K. Nanda†, and S. Satpathy
Department of Physics & Astronomy, University of Missouri, Columbia, MO 65211
(Dated: August 8, 2012)

We show that the substitutional vacancy in graphene forms a dynamical Jahn-Teller center. The adiabatic potential surface resulting from the electron-lattice coupling was computed using density-functional methods and subsequently the Schrödinger equation was solved for the nuclear motion. Our calculations show a large tunneling splitting 3Γ estimated to be about 64 cm^{-1}. The effect results in a large delocalization of the carbon nuclear wave functions around the vacancy leading to a significant broadening of the Jahn-Teller active $sp^2\sigma$ electron states. The tunneling splitting should be observable in electron paramagnetic resonance and two-photon resonance scattering experiments.

PACS numbers: 81.05.ue, 71.70.Ej, 31.30.-i

I. INTRODUCTION

In spite of its deceptively simple honeycomb lattice structure, graphene has quickly become a new paradigm for testing a variety of ideas in condensed matter physics. The much celebrated linear band structure of graphene[1] leads to a host of unusual behaviors[2–5] such as Klein tunneling, chiral electrons, minimum conductivity, negative refraction, half-integer quantum Hall effect, and new features in the Kondo and RKKY interactions.[6,7] Vacancies in the carbon based systems have been of considerable interest for quite some time now, especially in the context of magnetism without magnetic atoms.[8–14] Quite remarkably, it has been shown that a vacancy introduces a quasi-localized midgap state in the π bands with $\sim 1/r$ decay on account of the particle-hole symmetry.[9,15] An interesting consequence of this is the partial occupation of the vacancy-induced σ-band states, which leads then to a Jahn-Teller (JT) distortion. The JT distortion could be static or dynamic. In the latter, the potential barrier between the different equivalent minima in the nuclear configuration space is small enough that the nuclei tunnel between the various minima leading to several interesting effects, while in the static JT effect, the nuclei are stuck to one minima or the other. In this paper, we show that the vacancy forms a dynamical JT center in graphene owing to the small quantum mechanical barrier for nuclear tunneling.

II. JAHN-TELLER COUPLING AND THE ADIABATIC POTENTIAL SURFACE

Density-functional calculations[9] show that the vacancy introduces four electrons into the graphene bands as illustrated in Fig. 1. The JT effect comes from the partial occupation of the doubly-degenerate $sp^2\sigma$ dangling bond states on the carbon triangle surrounding the vacancy and their coupling to the two vibrational modes of the triangle, given by the $E\otimes e$ JT Hamiltonian[17]

$$\begin{aligned}\mathcal{H} &= -\frac{\hbar^2}{2M}\left(\frac{\partial^2}{\partial Q_1^2}+\frac{\partial^2}{\partial Q_2^2}\right)+\frac{1}{2}K\left(Q_1^2+Q_2^2\right) \\ &+ g\left(Q_1\hat{\tau}_z+Q_2\hat{\tau}_x\right)+G\left[\left(Q_1^2-Q_2^2\right)\hat{\tau}_z+2Q_1Q_2\hat{\tau}_x\right],\end{aligned} \tag{1}$$

where the terms are the nuclear kinetic energy, the elastic energy, and the linear and the quadratic JT coupling terms. Here the pseudospin $\vec{\tau}$ describes the two JT active, doubly-degenerate electronic states $|v_1\rangle$ and $|v_2\rangle$ originating from the three $sp^2\sigma$ dangling bonds on the carbon triangle: $|v_0\rangle = (\sigma_1+\sigma_2+\sigma_3)/\sqrt{3}$, $|v_1\rangle = (-\sigma_2+\sigma_3)/\sqrt{2}$, $|v_2\rangle = (2\sigma_1-\sigma_2-\sigma_3)/\sqrt{6}$, with energies $E_0=-2t$ and $E_{1,2}=t$ and symmetries A_1 and E, respectively, with the $-t$ being the σ-electron hopping between the neighboring sites on the triangle, and $|v_1\rangle$ transforms like x and $|v_2\rangle$ like y. On the other hand, the p_z orbitals, responsible for the linear 'π' Dirac bands, introduce the quasi-localized midgap state, which becomes singly-occupied due to Hund's coupling, leaving a lone electron to occupy the σ-derived doubly-degenerate E state. This explains the relative positions of the vacancy states shown in Fig. 1. Density-functional calculations yield a net magnetic moment of about $1.7\mu_B$ and may be understood as follows. The Hund's-rule coupling between the Vσ and Vπ electrons leads to a $S=1$ state with a magnetic moment of $2\mu_B$, which is reduced by about $0.3\mu_B$ due to the anti-ferromagnetic spin-polarization of the π band itinerant states in the vicinity of the vacancy as schematically illustrated in Fig. 1.

Turning now to the three vibrational modes of the triangle: $|Q_0\rangle = (0,2,\sqrt{3},-1,-\sqrt{3},-1)/\sqrt{12}$, $|Q_1\rangle = (0,2,-\sqrt{3},-1,\sqrt{3},-1)/\sqrt{12}$, $|Q_2\rangle = (2,0,-1,\sqrt{3},-1,-\sqrt{3})/\sqrt{12}$,[17] Q_0 is the stretching mode and the doubly-degenerate Q_1 and Q_2 modes are JT active, splitting the upper two Vσ bands as shown in Fig. 1. The parameters in the Hamiltonian are the carbon mass M, the elastic energy K, and the linear and quadratic JT coupling parameters g and G, respectively. Diagonalization of the potential terms in Eq. 1 leads to the well-known adiabatic potential surface (APS) for the nuclear motion

$$E_\pm = \frac{1}{2}K\rho^2 \pm \rho\sqrt{g^2+G^2\rho^2+2gG\rho\cos(3\phi)}, \tag{2}$$

where $\rho = \sqrt{Q_1^2 + Q_2^2}$ and $\phi = \tan^{-1}(Q_2/Q_1)$ are the polar coordinates and $E_\pm$ denote the two potential sheets. Without the quadratic coupling ($G = 0$), one gets the Mexican hat APS, while with it we have three minima in the (Q_1, Q_2) space (Fig. 2). The electronic eigenfunction for the lower sheet is[17]

$$|\psi^e\rangle = [\sin(\phi/2)|v_1\rangle + \cos(\phi/2)|v_2\rangle] \times e^{i\phi/2}, \quad (3)$$

where the phase factor assures single-valuedness as one moves around the origin and leads to a Berry phase.

III. DENSITY-FUNCTIONAL COMPUTATION OF THE ADIABATIC POTENTIAL SURFACE

In order to study the APS, we have computed the total energy as a function of the vibronic coordinates using the spin-polarized density functional all-electron linear augmented plane-waves (LAPW) method[20] and the gradient approximation (GGA) for the exchange-correlation functional.[21] We used a 32-atom supercell with a single vacancy and obtained a fully relaxed structure, which yielded a planar structure with an isosceles triangle for the carbon atoms surrounding the vacancy with two long bonds (2.66 Å) and one short bond (2.41 Å). This is equivalent to the distortion: $Q_0 = 0.08$ Å, $Q_1 = 0.166$ Å, and $Q_2 = 0$. We then took a series of structures with varying distortions, Q_1 and Q_2, and in each case optimized the rest of the carbon atoms in the supercell. We note that while the literature is divided regarding whether the relaxed structure with a vacancy is planar or non-planar, the three-fold symmetry of the adiabatic potential surface occurs in either case, being tied to the symmetry of the honeycomb lattice itself. Throughout the calculations, the atomic sphere radius ($R_{\rm MT}$) was fixed at 0.63 Å, while the LAPW basis functions were cutoff at $RK_{max} = 4.6$, with approximately 3500 basis functions at each $\mathbf{k}$ point, and we retained the angular momentum expansion inside the atomic sphere up to $l_{max} = 6$. The basis set included $2s$, $2p$ valence functions for the C atoms.

The calculated energies are shown in Fig. 2, which yields the JT distortion radius $\rho_0 = 0.165$ Å, the JT stabilization energy $E_{\rm JT}$= 110 meV and the tunneling barrier height β=19 meV. Comparison of these results with Eq. (2) yields the stiffness constant $K = 9.3\ eV/$ Å^2 and the linear and the quadratic JT parameters $g = 1.46\ eV/$ Å and $G = 0.38\ eV/$ Å^2, respectively. For the case of $LaMnO_3$, a well-known system with a strong JT interaction, while the K and g are about the same, the warping parameter $G = 2.0\ eV/$ Å^2 is significantly large,[22] which results in a static JT effect with the nuclei stuck to one potential minimum. In contrast, the weaker warping term G in graphene leads to a small barrier height for nuclear tunneling and consequently to the dynamic JT effect, where the nuclei tunnel between the three minima in the APS.

IV. TIGHT-BINDING NUCLEAR HOPPING AND THE BERRY PHASE

The basic features of the collective nuclear-electronic motion may be described by adopting a simple tight-binding approach, familiar from the electronic structure theory. We write the collective wave function as the linear combination $|\Psi\rangle = c_1\ \phi_1(R)\ \psi_1^e(R,r) + c_2\ \phi_2(R)\ \psi_2^e(R,r) + c_3\ \phi_3(R)\ \psi_3^e(R,r)$, where $R(r)$ is the nuclear (electronic) coordinate, $\phi_i(R)$ solves the nuclear Schrödinger equation in the vicinity of the potential minima,

$$[T_R + V_i(R)]\phi_i(R) = E_0\phi_i(R), \quad (4)$$

and $\psi_i^e(R,r)$ satisfies the electronic Schrödinger equation for the fixed nuclear position $R \equiv (Q_1, Q_2)$. The electronic wave function is restricted to the Hilbert space $(|v_1\rangle, |v_2\rangle)$ and has the form Eq. (3) for a given nuclear coordinate R. Thus the energy eigenstates assume the Born-Oppenheimer form $|\Psi(R)\rangle = \Phi_n(R)|\psi_e(R,r)\rangle$, where $\Phi_n(R) = c_1\phi_1(R) + c_2\phi_2(R) + c_3\phi_3(R)$ is a linear combination of the nuclear orbitals.

The eigenstates can then be obtained from the diagonalization of the 3×3 tight-binding Hamiltonian

$$H = \begin{pmatrix} E_0 & \Gamma e^{i\phi} & \Gamma e^{-i\phi} \\ \Gamma e^{-i\phi} & E_0 & \Gamma e^{i\phi} \\ \Gamma e^{i\phi} & \Gamma e^{-i\phi} & E_0 \end{pmatrix}, \quad (5)$$

where the phase factor $e^{i\phi}$ will be discussed momentarily, E_0 is the on-site energy, and Γ is the nuclear hopping integral in the adiabatic approximation $\Gamma = \langle\phi_1(R)\psi^e(R,r)|\Delta V(R)|\phi_2(R)\psi^e(R,r)\rangle \approx -\Delta V \times F$. In obtaining the last result, the normalization $\langle\psi^e(R,r)|\psi^e(R,r)\rangle = 1$ has been used,

$$F = \int \phi_1^*(R)\phi_2(R)d^3R \quad (6)$$

is the Frank-Condon factor, and the deviation of the lower APS potential from the well potential, $\Delta V(R) = V_-(R) - V_i(R)$, has been approximated by its value $-\Delta V$ at the saddle point (marked by a cross in the bottom panel in Fig (2)), since that's where most of the contribution to the integral comes from.

The magnitude of the nuclear hopping Γ may be estimated by assuming a one-dimensional motion of the nuclei in the azimuthal direction, along the circle of radius ρ_0 and by computing the quantities ΔV and F. The 1D motion is reasonable since by expanding the adiabatic potential V_- around the potential minima, the spring constant for azimuthal motion is found to be $K' = 9G$, which is about half of the spring constant K for radial motion. This corresponds to a phonon frequency of $\hbar\omega \approx 58$ meV for radial motion and ≈ 34 meV for the azimuthal motion. The latter is of the same order of magnitude as the tunneling barrier of 19 meV, which again indicates strong tunneling between the three minima. Now, taking

the nuclear wave functions as the 1D simple harmonic oscillator wave function localized at the potential minima: $\phi(x) = (\pi l^2)^{-1/4} \exp\,[-x^2/(2l^2)]$, where $l = \hbar/\sqrt{MK'}$ and x is the length along the azimuthal direction, the Frank-Condon factor becomes simply the overlap integral between two displaced harmonic oscillator wave functions, with the result: $F = 2^{-1/2} \exp\,[-a^2/(4l^2)]$, where $a = 2\pi\rho_0/3$ is the distance between two minima along the circle. Meanwhile, the potential difference between the minimum and the saddle point can be found to be $\Delta V = \rho_0^2 \times (\pi^2 K'/18 - 2G)$. Plugging in the numerical values, we find $F \simeq 0.13$ and $\Delta V \simeq 0.035$ eV, so that the hopping integral $\Gamma \approx \Delta V \times F = -37$ cm^{-1}.

Finally, in addition to the hopping integral, the adiabatic motion of the electron results in a fictitious magnetic field seen by the nuclei with the vector potential[23]

$$\vec{A} = -\frac{\hbar}{q}\, \mathrm{Im}\langle\psi_e(R,r)|\vec{\nabla}_R\psi_e(R,r)\rangle, \tag{7}$$

which adds a phase factor, the Berry phase, to the hopping amplitude in the Hamiltonian (5). The modified hopping in the presence of the magnetic field, from point a to b, is given by the expression[24]

$$\Gamma = \Gamma_{\vec{A}=0} \times \exp\,[\,\frac{iq}{\hbar}\int_a^b \vec{A}\cdot d\vec{s}\,]. \tag{8}$$

It immediately follows from Eqs. (3) and (7) that $\vec{A} = -2^{-1}\hbar q^{-1}\hat{e}_\phi$, so that the phase factor in Eq. (8) is simply $e^{i\phi} = e^{i\pi/3}$. This phase factor, the Berry phase, is very important as without this, the symmetry of the ground state is incorrectly predicted. Diagonalization of the Hamiltonian Eq. (5) with the correct phase factor yields a doubly-degenerate nuclear ground-state with energy Γ, with the singly-degenerate excited state at energy -2Γ, so that the energy separation is $3|\Gamma| = 111$ cm^{-1}.

This crude but conceptually rich tight-binding result may be compared to the exact, brute-force diagonalization of the full Hamiltonian Eq. (1) by expanding the combined nuclear-electronic wave function $|\Psi\rangle$ in a complete basis set[17,25]

$$\begin{aligned} |\Psi\rangle \;=\; & \sum_{n=0}^{N}\sum_{m=0}^{N-n}\Bigg[A_{nm}\frac{(c_1^\dagger)^n}{\sqrt{n!}}\frac{(c_2^\dagger)^m}{\sqrt{m!}}|0\rangle|v_1\rangle \\ & +\; B_{nm}\frac{(c_1^\dagger)^n}{\sqrt{n!}}\frac{(c_2^\dagger)^m}{\sqrt{m!}}|0\rangle|v_2\rangle\Bigg], \end{aligned} \tag{9}$$

where $c_1^\dagger, c_2^\dagger$ create harmonic oscillator states along the Q_1, Q_2 axes centered at the origin and A_{nm} and B_{nm} are the expansion coefficients. This procedure requires no additional consideration of a fictitious magnetic field and also yields the full solutions in addition to the lowest three states obtained from the tight-binding theory. The results are shown in Fig. (3). The tunneling splitting obtained from the difference between the ground and the excited state energies has the magnitude $3|\Gamma| = 86$ cm^{-1}, which compares very well with the tight-binding result.

V. NUCLEAR WAVE FUNCTION

The nuclear probability density in the configuration space (Q_1, Q_2) may be written as

$$|\Psi_N(Q_1,Q_2)|^2 = \sum_{nm}(|A_{nm}|^2+|B_{nm}|^2)|\phi_n(Q_1)|^2|\phi_m(Q_2)|^2, \tag{10}$$

where ϕ_n is the nth harmonic oscillator eigenfunction and the expansion coefficients A_{nm} and B_{nm} are obtained from the solution of Eq. 9. The results for the ground state, shown in Fig. (4), indicate the confinement of the nuclear wave function at the three minima of the APS with a significant component in the barrier region in between the minima.

The real space wave function $|\Psi_N(r)|^2$ can be computed from the corresponding quantity $|\Psi_N(Q_1,Q_2)|^2$ in the configuration space. The result is shown in Fig. (5), which indicates a significant spread of the nuclear wave function of the carbon triangle, about 0.1 Å from the equilibrium positions. We note that this is not washed out by the lattice thermal vibrations, which causes the nuclear vibrational amplitude, estimated from the expression $\frac{1}{2}KQ^2 = \frac{3}{2}k_BT$ to be about 0.05 Å at room temperature.

The spread of the nuclear wave function broadens the energy of the JT split electronic states as well, so that they are not sharp δ-function states any longer. In the adiabatic approximation, the electronic density-of-states is given by $\rho(E) = \sum_{Q_1Q_2}|\Psi_N(Q_1,Q_2)|^2 \times [\delta(E - \varepsilon_-(Q_1,Q_2)) + \delta(E - \varepsilon_+(Q_1,Q_2))$, where $\varepsilon_\pm$ denote the energies of the two JT split states in the expression (2) but without the elastic energy term. The results are shown in the inset of Fig. (5), which predicts a rather large width, of the order of 0.20 eV, due to the JT effect. Thus these states should appear as rather broad states in the density-of-states. In contrast to this, the broadening of the midgap $V\pi$ state is expected to be rather small. In fact, it is exactly zero if only the nearest-neighbor hopping is retained.[15] This is borne out by the less than 5 meV width of the midgap state, seen in the scanning tunneling experiments.[16]

VI. DISCUSSIONS

The above analysis included just one pair of vibrational modes Q_1 and Q_2 corresponding to the atoms in the first shell around the vacancy as described in the Hamiltonian Eq. 1. There are more such modes corresponding to the farther shells. For instance, there is also a pair of modes in the second shell[26] and so on. It is difficult to treat the JT problem when multiple vibrational modes are present (the so-called multimode problem[27–29]) and often the single-mode approximation is made.[18,19] In the present case, due to the localized nature of the JT-active states (dangling sp^2 bond orbitals on the first shell atoms), the JT coupling to modes be-

longing to further neighbor shells is expected to be quite weak. The coupling is further weakened because of the small hybridization between the σ and the π states; In fact, the coupling is strictly forbidden by symmetry for the planar structure. As a result, the coupling of the vibronic modes belonging to the higher neighbor shells to the JT-active electronic states is only indirect, viz., via the structural relaxation of the first shell atoms. To study this, we have computed the vibronic coupling parameter g' for the Q_1 and Q_2 modes of the second shell atoms[26] from the density-functional calculations, which confirms that even for the second shell, the coupling is already quite small with $g' \approx g/6$. This being the case, the single-mode approximation should be accurate and it captures the essential physics in the present case.

A second point is that even in the single-mode problem, since all atoms in the crystal are involved in the vibration, the effective mass of the vibrational mode is not just the mass of the carbon atom as used above, but could be several times larger. The effective mass is given by the expression $1/2M_{eff}\dot{Q}^2 = 1/2M\sum_i(\dot{x}_i^2 + \dot{y}_i^2)$, where M is the atomic mass, the summation goes over all atoms in the solid, and x_i, y_i represent the displacements for the given vibronic amplitude Q. If just the first shell is retained, then M_{eff} simply equals M, which follows from the normalization convention of the vibronic modes with respect to the first shell of atoms. The displacements of the atoms fall off rapidly with distance from the vacancy, e.g., as $1/r^2$ for 3D and $1/r$ for 2D lattices within the linear elastic continuum theory,[30] so that most of the contribution to the effective mass should come from the first few shells.

From our density-functional calculations, we can estimate the effective mass if we neglect the contributions of the shells beyond the fifth shell. The effective mass is estimated from the expression $M_{eff} = \sum_m M_m$, where $M_m = \nu_m \times (\Delta r_m/\Delta Q)^2$ is the contribution to the effective mass from the m^{th} shell, ν_m is the number of atoms, and $\Delta r_m = \langle[(\Delta x)^2 + (\Delta y)^2]\rangle^{1/2}$ is the average deviation of the positions of the atoms belonging to the m^{th} shell. In deriving this expression, we have made the linear approximation, valid for small oscillations, viz., that $\dot{Q}/\dot{x}_i \approx Q/x_i$, etc. The results listed in Table I show that the contribution to the effective mass rapidly converges with the shell distance, yielding the value $M_{eff} \approx 1.8M$. The higher mass would reduce the tunneling splitting by the factor $(M_{eff}/M)^{1/2}$, so that $3|\Gamma| \approx 64$ cm^{-1} instead of the 86 cm^{-1} value computed earlier using the bare mass M.

The large value of the tunneling splitting as compared to the strain splitting, the typical value of which[31] is $\delta \sim 10$ cm^{-1}, results in the delocalization of the nuclear wave function. If the reverse were true, then the nuclei would be more or less stuck in one or the other potential well due to the removal of the degeneracy of the three APS minima by the local strain caused by the invariable presence of defects. This would therefore lead to a static distortion of the nuclear framework resulting in the static JT effect. For the dynamical JT effect, the tunneling splitting must be strong enough to overcome the strain splitting, so that the nuclei can tunnel between all APS minima, which is the case for graphene.

VII. CONCLUSION

In conclusion, we showed that the substitutional vacancy in graphene forms a dynamical JT center owing to a weak potential barrier for tunneling between the three minima in the adiabatic potential surface. The doubly-degenerate nuclear ground state with the tunneling splitting of about 64 cm^{-1} originates from the combined nuclear-electronic motion, which may be cast in terms of a Berry phase acquired due to a fictitious magnetic field experienced by the nuclei caused by the adiabatic motion of the electrons. The splitting should be observable in the electron paramagnetic resonance and two-photon resonance scattering experiments, which have been used to study the JT effects in the triatomic molecules. The quantum mechanical spread of the nuclear wave function is predicted to lead to a significant broadening of the JT split dangling bond states. Recently, it has been proposed[32] that the entanglement between the nuclear and electronic motion in a dynamical JT system may be exploited in quantum computation, leading to the possibility of yet another novel application for graphene.

This work was supported by the U. S. Department of Energy through Grant No. DE-FG02-00ER45818.

* Permanent Address: Institute of Nuclear Sciences, Vinča, University of Belgrade, P. O. Box 522, 11001 Belgrade, Serbia

† Permanent Address: Department of Physics, Indian Institute of Technology Madras, Chennai 600036, India

[1] P. R. Wallace, Phys. Rev. **71**, 622 (1947).
[2] K. S. Novoselov, A. K. Geim, S. V. Morozov, D. Jiang, Y. Zhang, S. V. Dubonos, I. V. Grigorieva, A. A. Firsov, Science **306**, 666-669 (2004).
[3] A. H. Castro Neto, F. Guinea, N. M. R. Peres, K. S. Novoselov, and A. K. Geim, Rev. Mod. Phys. **81**, 109 (2009).
[4] D. S. L. Abergel, V. Apalkov, J. Berashevich, K. Ziegler, and T. Chakraborty, Adv. Phys. **59: 4** 261 (2010).
[5] S. Das Sarma, S. Adam, E. H. Hwang, and E. Rossi, Rev. Mod. Phys. **83**, 407 (2011).
[6] M. Sherafati and S. Satpathy, Phys. Rev. B **83**, 165425 (2011).
[7] M. Sherafati and S. Satpathy, Phys. Rev. B **84**, 125416 (2011).
[8] A. V. Krasheninnikov and K. Nordlund, J. Appl. Phys.

107, 071301 (2010).
[9] B. R. K. Nanda, M. Sherafati, Z. Popović, and S. Satpathy, New J. Phys. **14**, 083 004 (2012).
[10] P. Esquinazi, D. Spemann, R. Höhne, A. Setzer, K. -H. Han, and T. Butz, Phys. Rev. Lett. **91**, 227201 (2003).
[11] J. Barzola-Quiquia, P. Esquinazi, M. Rothermel, D. Spemann, T. Butz, and N. Garcia, Phys. Rev. B **76**, 161403(R) (2007).
[12] R. Faccio, L. Fernandez-Werner, H. Pardo, C. Goyenola, O. N. Ventura, and A. W. Mombru, J. Phys. Chem. C **114**, 18961 (2010).
[13] P. O. Lehtinen, A. S. Foster, Y. Ma, A. V. Krasheninnikov, and. R. M. Nieminen, Phys. Rev. Lett. **93**, 187202 (2004).
[14] R. R. Nair, M. Sepioni, I-Ling Tsai, O. Lehtinen, J. Keinonen, A. V. Krasheninnikov, T. Thomson, A. K. Geim, and I. V. Grigorieva, Nat. Phys. Letts. **8**, 199 (2012).
[15] V. M. Pereira, J. M. B. Lopes dos Santos, and A. H. Castro Neto, Phys. Rev. B **77**, 115109 (2008).
[16] M. M. Ugeda, I. Brihuega, F. Guinea, and J. M. Gómez-Rodríguez, Phys. Rev. Lett. **104**, 096804 (2010).
[17] I. B. Bersuker, *The Jahn-Teller Effect* (Cambridge University Press, 2006).
[18] P. Gaciá-Fernández, A. Trueba, M. T. Barriuso, J. A. Aramburu, and M. Moreno, Phys. Rev. Lett. **104**, 035901 (2010).
[19] T. A. Abtew, Y. Y. Sun, B.-C. Shih, P. Dev, S. B. Zhang, and P. Zhang, Phys. Rev. Lett. **107**, 146403 (2011).
[20] P. Blaha, K. Schwarz, G. K. H. Madsen, D. Kvasnicka and J. Luitz, WIEN2k, An Augmented Plane Wave + Local Orbitals Program for Calculating Crystal Properties (Karlheinz Schwarz, Techn. Universitat Wien, Austria), 2001. ISBN 3-9501031-1-2.
[21] J. P. Perdew, S. Burke, and M. Ernzerhof, Phys. Rev. Lett. **77**, 3865-3868 (1996).
[22] Z. S. Popović and S. Satpathy, Phys. Rev. Lett. **84**, 1603 (2000).
[23] C. A. Mead, Rev. Mod. Phys. **64**, 51 (1992).
[24] See, for example, "The Feynman Lectures on Physics," R. Feynman, R. B. Leighton, and M. L. Sands, (Addison-Wesley, Reading, Massachusetts, 1963).
[25] V. Perebeinos, P. B. Allen, and M. Pederson, Phys. Rev. A **72**, 012501 (2005).
[26] A. D. Liehr, Annu. Rev. Phys. Chem. **13**, 41 (1962).
[27] M. C. M. O'Brien. J. Phys. C: Solid State Phys. **5** 2045 (1972).
[28] I. B. Bersuker and V. Z. Polinger, *Vibronic Interactions in Molecules and Crystals* , Springer-Verlag, Berlin (1989).
[29] M. Zlatar, J.-P. Brog, A. Tschannen, M. Gruden-Pavlović, and C. Daul, in *Vibronic Interactions and the Jahn-Teller Effect*, Prog. Theor. Chem. and Physics **B23**, Eds: M. Atanasov, C. Daul, and P. L. W. Tregenna-Piggott (Springer, 2012).
[30] See, for example, E. H. Brandt, Phys. Rev. B **56**, 9071 (1997) and references therein.
[31] F. S. Ham, in *Electron Paramagnetic Resonance*, edited by S. Geschwind (Plenum, New York, 1972).
[32] R. Englman and T. Vértesi, J. Chem. Phys. **125**, 064102 (2006); A. P. Hines, C. M. Dawson, R. H. McKenzie, and G. J. Milburn, Phys. Rev. A **70**, 022 303 (2004).

Figures

FIG. 1: (Color online) Vacancy induced σ and π electron states (V_σ and V_π) with the occupied states shown by dots with arrows (*left*). The nominal $2\mu_B$ ($S = 1$) magnetic moment due to the localized states is reduced substantially due to the anti-ferromagnetic spin polarization of the band states, indicated by $\pi_l \uparrow\downarrow$, in the local neighborhood of the vacancy. *Right* part shows the JT active electron states, $|v_1\rangle$ and $|v_2\rangle$, and the vibrational modes of the carbon triangle that they couple to. σ_i denotes the dangling $sp^2\sigma$ bond orbital on a carbon atom adjacent to the vacancy.

FIG. 2: (Color online) Total energy as a function of the vibronic distortion Q_1 computed from the DFT (red dots) and fitted to the adiabatic energy E_- in Eq. (2)(full line) *(Top)*. Shown also are the computed JT stabilization energy E_{JT}, the barrier height β for nuclear tunneling, and the magnitude of the JT distortion ρ_0. The triangles indicate the configurations at the three extrema. *Bottom* figure shows the corresponding energy contours in the $Q_1 - Q_2$ plane (the adiabatic potential surface), with the three equivalent minima (dots) separated by the tunneling barriers (crosses). The contour values are: $-0.11 + 0.001 \times (2^n)$ in units of eV, where $n = 0, 1, ..., 7$ labels the contours and Γ denotes the nuclear hopping integral in the tight binding description.

FIG. 3: (Color online) Eigenvalues obtained by diagonalization of Eq. (1) using the basis set Eq. (9) as a function of the scaled coupling strengths λg and λG. Numbers inside the figure indicates the degeneracies. For $\lambda = 0$, eigenstates of the two-dimensional harmonic oscillator are reproduced.

FIG. 4: (Color online) Nuclear ground-state probability density $|\Psi_N(Q_1, Q_2)|^2$ in the configuration space, indicating the localization of the wave function near the three minima of the adiabatic potential surface.

FIG. 5: (Color online) Nuclear probability density $|\Psi_N(r)|^2$ in the ground state showing the symmetric distortion of the carbon atoms from the ideal position of an equilateral triangle (solid line). The nuclei move in a correlated manner so that the most probable configuration is one of the three isosceles triangles (one of which is indicated by the dashed lines) corresponding to the three minima of the APS. The nuclear motion of the nearby atoms show much smaller deviation from their equilibrium positions. The *inset* shows a significant broadening, computed within the adiabatic approximation, of the JT active electron states due to the spread of the nuclear wave function.

Tables

TABLE I: Average displacement of a carbon atom Δr_m (in Å) in the m^{th} shell surrounding the vacancy for the JT distortion $Q_1 = 0.24$ Å. ν_m denotes the number of atoms in the shell and M_m is the shell contribution of the effective mass.

Shell no. (m)	1	2	3	4	5
ν_m	3	6	3	6	3
$\lvert\Delta r_m\rvert$	0.139	0.072	0.055	0.033	0.021
M_m	1.00	0.53	0.15	0.11	0.02

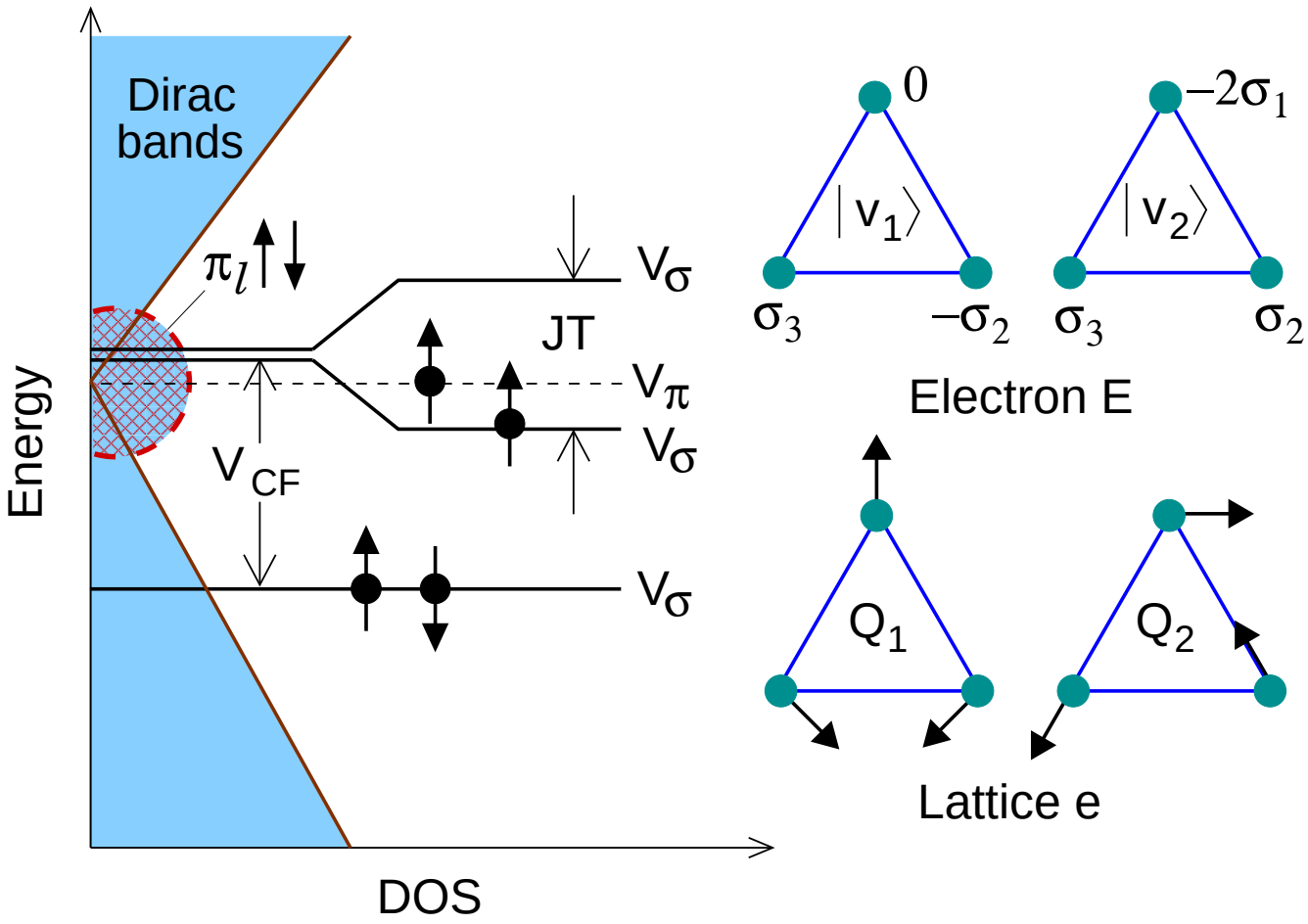

Figure 1 LR13154 08Aug2012

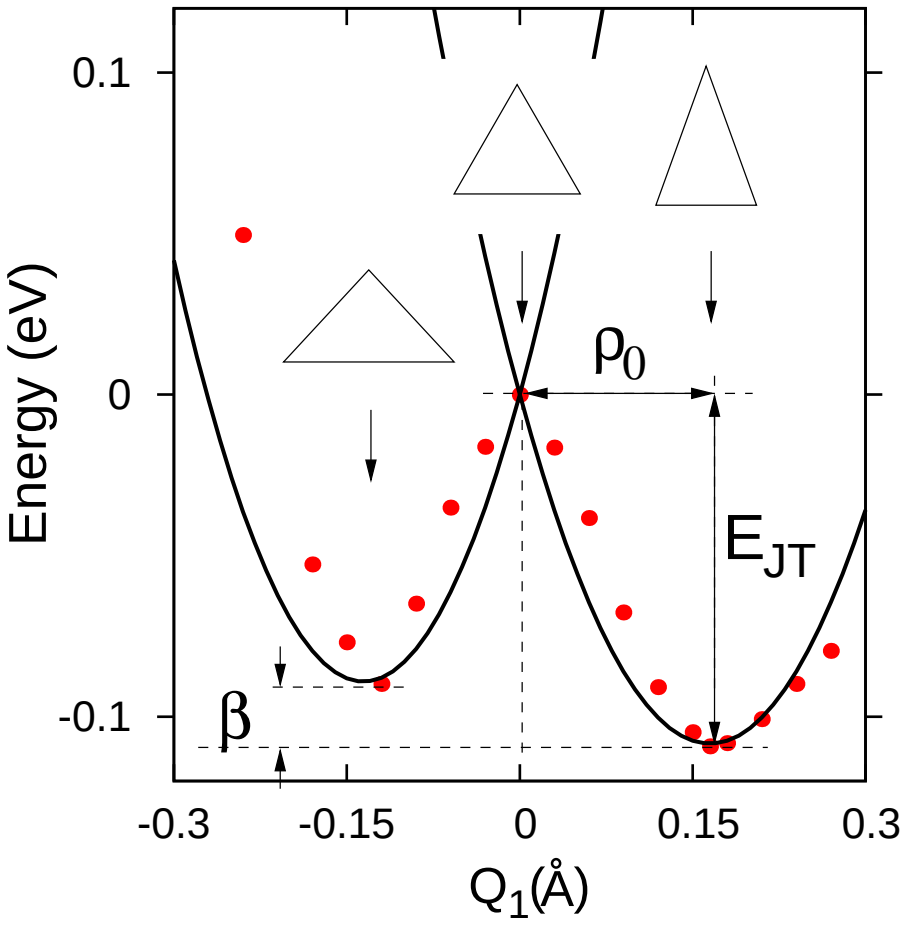

Figure 2a LR13154 08Aug2012

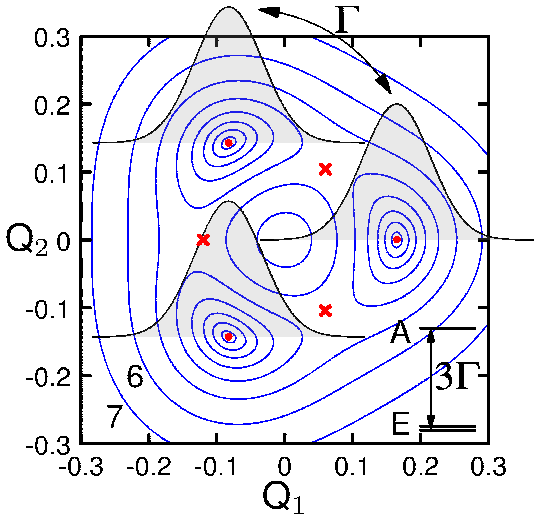

Figure 2b LR13154 08Aug2012

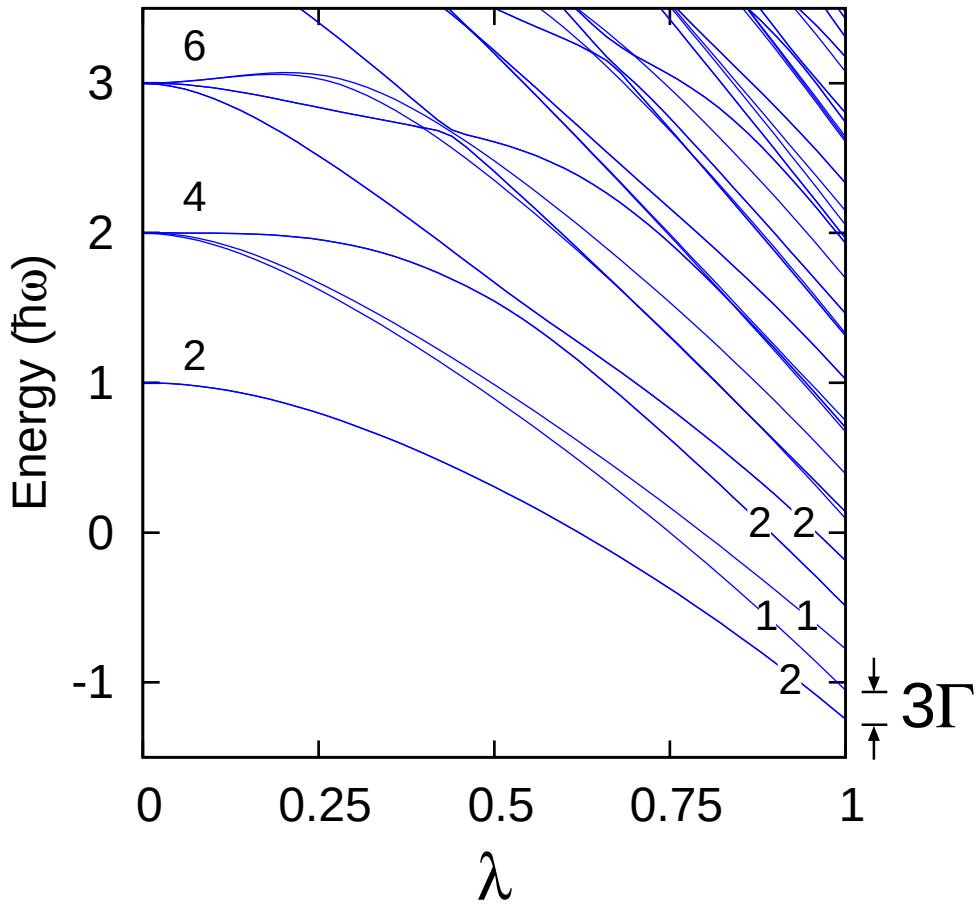

Figure 3 LR13154 08Aug2012

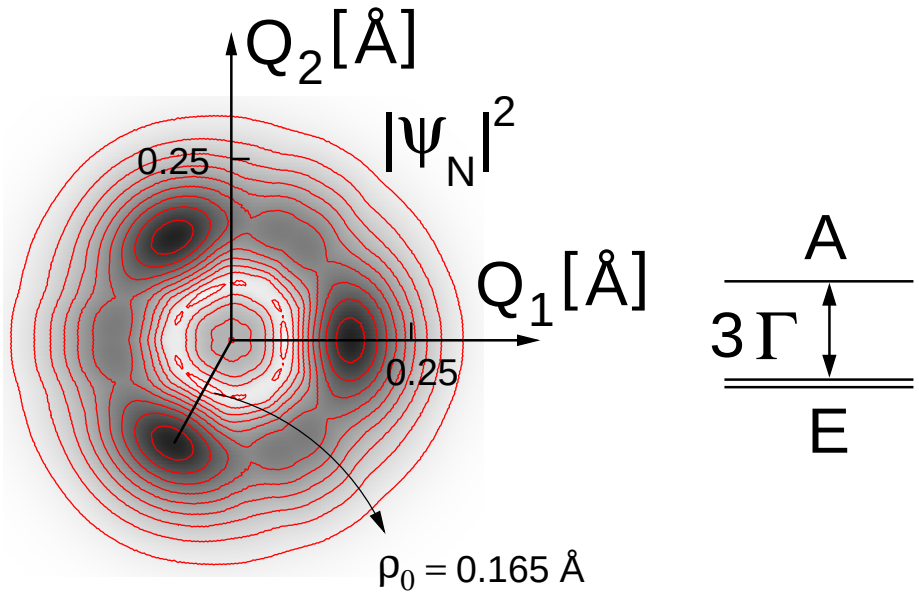

Figure 4 LR13154 08Aug2012

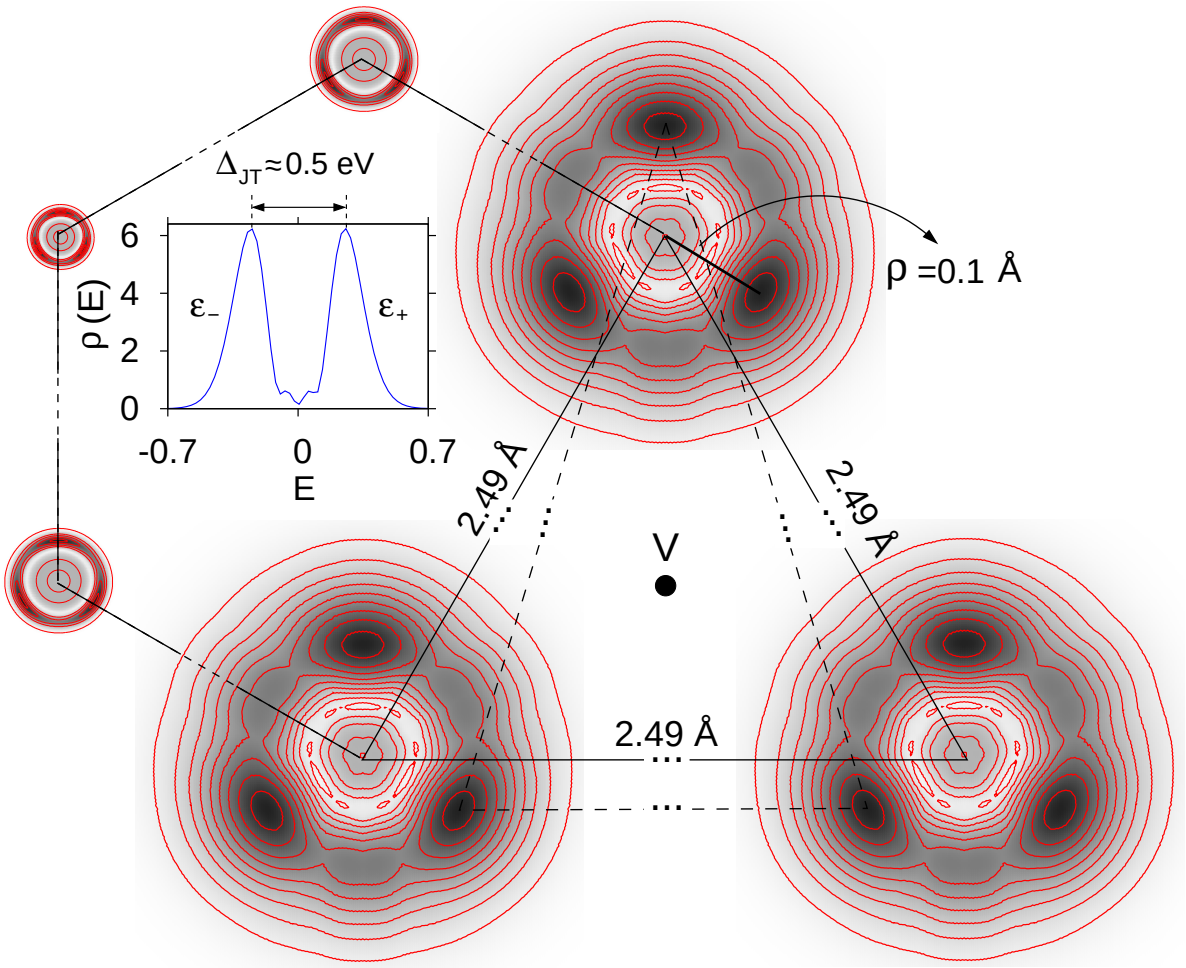

Figure 5 LR13154 08Aug2012